Polymer 50 (2009) 1324–1332

Contents lists available at ScienceDirect

Polymer

journal homepage: www.elsevier.com/locate/polymer

Molecular dynamics simulation of mixed matrix nanocomposites containing polyimide and polyhedral oligomeric silsesquioxane (POSS)

Yin Yani, Monica H. Lamm*

Department of Chemical & Biological Engineering, Iowa State University, Ames, IA 50011, USA

ARTICLE INFO

Article history:
Received 20 August 2008
Received in revised form
22 December 2008
Accepted 23 December 2008
Available online 9 January 2009

Keywords:
Polyhedral oligomeric silsesquioxane
Polyimide
Molecular dynamics simulations

ABSTRACT

Mixed matrix blends containing polyimide (PI) and polyhedral oligomeric silsesquioxanes (POSS) are studied with atomistic molecular dynamics simulation. To examine the effect of functional group, two types of POSS are considered, either octahydrido silsesquioxane (OHS) or octaaminophenyl silsesquioxane (OAPS). The glass transition temperature of the model PI–OAPS blends increases with the incorporation of OAPS, an observation consistent with recent experiments on these systems. A decrease in glass transition temperature is shown for the model PI–OHS blends. Radial distribution functions for both blends are presented to show how packing between the inorganic (POSS) and organic (PI) species in the mixed matrix varies as a function of POSS loading and POSS functionalization. In addition, we report the mobility of the PI chains and POSS molecules in the material by calculating the mean square displacement. These results provide molecular insight about thermal property enhancements afforded by POSS-based additives.

1. Introduction

Membranes have been widely used in gas separation applications, such as for hydrogen purification, hydrogen recovery in oil refinery processes, air purification, and natural gas processing. Membranes were first introduced for gas separation by J.K. Mitchell of Philadelphia in 1831 [1]. The most commonly used membranes in industry are made from polymers. Polymeric membranes are cost effective, easy to process, and have good gas transport properties. The main drawback for this type of membrane is the inability to withstand elevated temperatures. At high temperatures, the mobility of individual polymer chains increases which results in poor selectivity for the membranes. Therefore, polymer membranes cannot be used to produce gases of high purity. Other types of membranes that have been used for gas separation are inorganic membranes. This type of membrane has good permeability and comparable selectivities for gases at elevated temperature. However, inorganic membranes are difficult to process and less cost effective compared to polymeric membranes. Therefore, attention has focused on the development of another type of membrane, mixed-matrix nanocomposites [2], which incorporate an inorganic molecular sieve within the polymeric matrix.

Mixed-matrix nanocomposites are a high performance material that combine the advantages of inorganic fillers and polymeric materials. Polyhedral oligomeric silsesquioxanes (POSSs) are one of the inorganic fillers that have been used for this purpose. POSS has the chemical composition of $(RSiO_{1.5})_n$ with R as an organic functional group. The possibility to synthesize POSS with different functional groups results in many potential application areas for POSS-based materials, for example, as additives to paints and coatings [3–5], as well as in packaging materials and advanced plastics where POSS enhances temperature resistance [6–9].

The functional groups on POSS may affect the physical properties such as melting point and crystal structure [8,10]. Thus, in order to determine these properties, many synthetic methods have been developed to explore how selected organics groups modify the properties of POSS [11,12]. Laine et al. [12] described methods of synthesizing POSS with liquid crystalline and polymerizable organic moieties. They synthesized octavinyldimethylsiloxy silsesquioxane and octahydridodimethylsiloxy silsesquioxane to produce material with well-defined microporosity and high surface area. The two different functional groups were able to produce materials with different pore size distribution.

The impact of functional group on POSS materials has also been studied computationally. Ionescu et al. [8] used molecular dynamics simulation to show that octahydrido silsesquioxane (OHS, R = H) yields a different crystal structure than the crystal structure of octamethyl silsesquioxane. Striolo et al. reported the molecular simulation results for the radial distribution function and the effective pair potentials of mean force between OHS and between octamethyl silsesquioxanes in normal hexadecane [13],

* Corresponding author. Tel.: +1 515 294 6533; fax: +1 515 294 2689.
E-mail address: mhlamm@iastate.edu (M.H. Lamm).

0032-3861/$ – see front matter © 2009 Elsevier Ltd. All rights reserved.
doi:10.1016/j.polymer.2008.12.045

poly(dimethylsiloxane) [13], and normal hexane [14] solvents; and between POSS–alkane telechelic hybrid monomers in normal hexane [15] solvent. Their results have shown that replacing the hydrogen atoms in OHS with methyl groups alters the effective POSS–POSS interactions.

POSS can be incorporated in polymers to form nanocomposite materials in different ways, such as by physically blending the POSS molecules with the polymer [10], by introducing them as pendant groups on the polymer chain [16,17], or by covalent binding within the polymer backbone [17,18]. The incorporation of POSS molecules into a polymer results in improved material properties such as increased thermal stability, increased glass transition temperature, improved heat resistance, and reduction in flammability and heat evolution [3,4,9,19,20]. Lee et al. [21], Leu et al. [22] and Chen et al. [23] have incorporated POSS into a polyimide polymer backbone for low dielectric film applications. POSS has also been incorporated as pendant groups in polynorbornene [24], methacrylate [25], poly-4-methylstyrene [26], polystyrene [27] and polyoxazolines [28]. In addition, some previous works have blended POSS with poly(methylvinylsiloxane) [29], poly(dimethylsiloxane) [10], and polystyrene [30].

Iyer and Coleman [31] studied blends of polyimide (PI) with octaphenyl silsesquioxane (OPS, $R = C_6H_5$) and with octaaminophenyl silsesquioxane (OAPS, $R = C_6H_4(NH_2)$). Their results for PI–OPS composites showed a visible phase separation at 5 wt% OPS loading. They have also shown that functionalizing OPS with amine groups enhanced thermal and mechanical stability of the composites. This was shown by higher glass transition temperatures found for the PI–OAPS composites compared to the pure PI. The higher glass transition temperature suggested favorable interactions between PI and OAPS. In their experiments, a transparent composite with well-dispersed OAPS was produced. They reported that good thermal stability of the composite was obtained with up to 20 wt% OAPS loading.

Although the number of experimental studies about the incorporation of POSS in polymeric materials has grown, there is still a lot more to understand concerning the effect of POSS on the thermal properties of the materials [17,32] and whether POSS molecules are disperse uniformly within the polymer or form aggregates [10,33,34]. In the last decade, molecular simulations have contributed to our knowledge about the fundamental interactions between polymer and POSS species. Bharadwaj et al. [16] studied the effects of POSS moieties onto polymeric chains as pendant groups using atomistic molecular dynamics simulations. They found out that the incorporation of POSS with cyclopentyl rings and POSS with cyclohexyl rings on polynorbornene chains lead to an increase in the glass transition temperature of the material. They have also shown that different functional groups on POSS affect how the polymer chain packed around the POSS molecules.

Striolo et al. [10] used molecular dynamics simulations to study the thermodynamic and transport properties of OHS and octamethyl ($R = CH_3$) silsesquioxanes dissolved in poly(dimethylsiloxane) (PDMS). Their results showed that POSS tend to attract to each other when dissolved in PDMS. Capaldi et al. [35] simulated blends of cyclopentyl-substituted POSS (CpPOSS) in a polyethylene (PE) matrix. They studied three different systems which contained 5, 15, and 25 wt% of CpPOSS. Their observation suggested a strong tendency of POSS particles to crystallize at room temperature. Patel et al. [36] conducted molecular dynamics simulations to study the effect of the incorporation of T_8, T_{10} and T_{12}-POSS monomers with various organic substituents onto the properties of polystyrene and poly(methyl methacrylate) (PMMA). In their study, POSS monomers were covalently bonded to the polymer matrix to form copolymer. Their results showed an increase in glass transition temperature with the incorporation of POSS in the polystyrene system, and a decrease in the glass transition temperature with the incorporation of POSS in the PMMA system.

In addition to the atomistic simulations discussed above, there is an alternative approach, called a coarse-grained (CG) model that has been used for POSS/polymer systems. A CG model eliminates the unimportant degrees of freedom in the simulation by treating a collection of atoms as one coarse-grained site, and therefore, larger systems can be considered at longer timescales. Chan et al. [37] have developed a CG model using a structural-based scheme to simulate self-assembly for nonyl-tethered POSS molecules dissolved in hexane solvent. Their results showed a small aggregate of POSS molecules, which is similar to the one obtained with atomistic simulations. They also reported that their CG model reduced computational time by about two orders of magnitude compared to simulations with the equivalent atomistic model.

Despite the above efforts, there are still a lot of unanswered questions about the formation and properties of POSS/polymer composites that need to be addressed, such as whether a different type of POSS will yield different thermodynamic

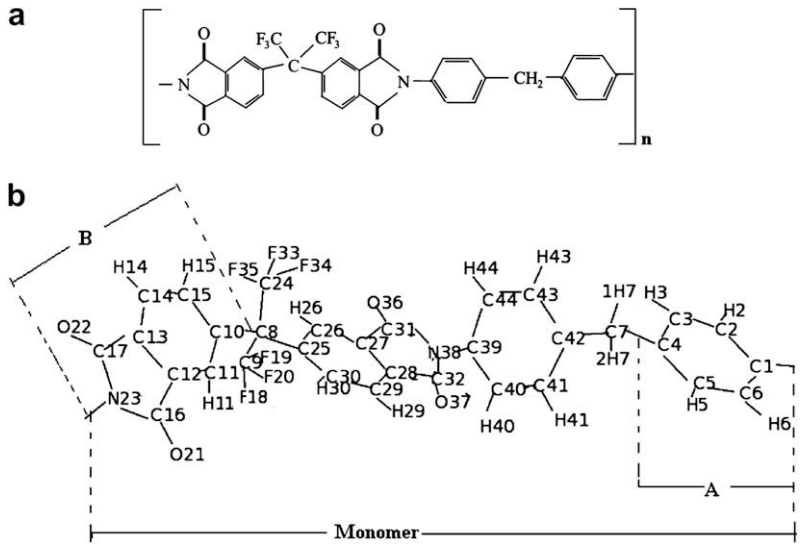

Fig. 1. (a) Repeat unit of the 6FDA-MDA polyimide polymer chain (b) Schematic to define the atom labels used with partial charges in Table 2.

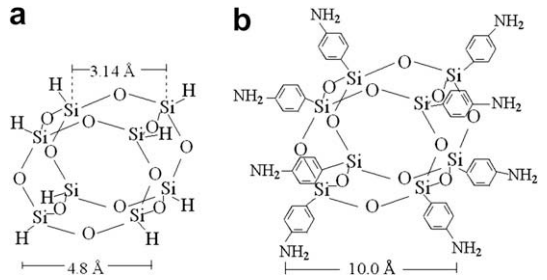

Fig. 2. Structures of simulated POSS (a) octahydrido silsesquioxanes (OHSs), (b) octaaminophenyl silsesquioxanes (OAPS).

properties for a POSS/polymer system, or whether a different loading of POSS will induce different packing of POSS and polymer in the material. In this work, we analyze the effect that incorporation of different POSS within a polyimide matrix has on the thermal properties of the nanocomposite. We provide a detailed molecular dynamics simulation study of POSS molecules blended with a polyimide (PI) polymer chain. Two types of POSS molecules will be considered: (i) POSS with hydrogen functional groups (OHS) and (ii) POSS with aminophenyl functional groups (OAPS). The paper is organized as follows: in Section 2, a detailed explanation of the force fields used in this work is provided and the molecular dynamics simulation method is explained; in Section 3, the simulation results are discussed and compared to the available experimental results; and in Section 4, a summary of the findings is provided.

Table 1
Parameters used in TRIPOS [38] force field for PI.

E_b	d_{ij}^0 (Å)	k_{ij} (kcal/mol Å^2)
C_{ar}–C_{ar}[a]	1.395	1400.0
C_{ar}–H	1.084	692.0
C–F	1.360	600.0
C–O	1.220	1555.2
C_{ar}–N	1.346	1305.94
C–C	1.540	633.6
C–C_{ar}	1.525	640.0
C–H	1.100	662.4
N–H	1.080	692.0
N–N	1.418	1300.0
E_θ	θ_0 (deg)	k_{ikj} (kcal/mol rad^2)
C_{ar}–C_{ar}–C_{ar}	120.0	78.79
C–C–H	109.5	52.52
F–C–F	109.5	131.31
C–C–C_{ar}	109.5	78.79
C_{ar}–C–C_{ar}	109.5	59.09
C–C_{ar}–C_{ar}	120.0	78.79
H–C–H	109.5	78.79
C_{ar}–N–C_{ar}	120.0	131.31
C_{ar}–C_{ar}–N	120.0	78.79
N–C–O	120.0	85.35
C–N–H	119.0	52.52
C–N–N	118.0	131.31
E_χ	k (kcal/mol Å^2)	
C_{ar}	480	
C	480	
N	120	
E_ϕ	k_{iklj} (kcal/mol)	s
C_{ar}–C–C–F	0.2	3
H–C_{ar}–C_{ar}–N	2.0	−2
H–N_{ar}–C_{ar}–O	1.6	−2
C_{ar}–C–C_{ar}–C_{ar}	0.12	−3
O–C–N–C	1.6	−2
E_{vdw}	σ_{ij} (Å)	ε_{ij} (kcal/mol Å^2)
C_{ar}–C_{ar}	3.03	0.107
H–H	2.673	0.042
N–N	2.762	0.095
O–O	2.71	0.116
F–F	2.62	0.109

[a] Aromatic carbon.

Table 2
Partial charges for atoms in the PI monomer.

Label	q	Label	q	Label	q	Label	q
C1	0.0774	C10	−0.0203	O22	−0.4822	F34	−0.1186
C2	−0.1910	C11	−0.0398	N23	−0.0715	F35	−0.1186
C3	−0.1295	C12	−0.0691	C24	0.3552	O36	−0.4777
C4	0.0451	C13	−0.0469	C25	−0.0092	O37	−0.4775
C5	−0.1295	C14	−0.1126	C26	−0.0468	N38	−0.0669
C6	−0.1910	C15	−0.1260	C27	−0.0604	C39	0.0718
H2	0.1627	C16	0.4581	C28	−0.0774	C40	−0.1958
H3	0.1304	C17	0.4864	C29	−0.1214	C41	−0.1260
H5	0.1304	H11	0.1362	C30	−0.1022	C42	0.0379
H6	0.1627	H14	0.1614	C31	0.4582	C43	−0.1260
C7	−0.0774	H15	0.1609	C32	0.5036	C44	−0.1958
1H7	0.0580	F18	−0.1186	H26	0.1409	H40	0.1640
2H7	0.0580	F19	−0.1186	H29	0.1647	H41	0.1350
C8	−0.1129	F20	−0.1186	H30	0.1525	H43	0.1350
C9	0.3552	O21	−0.4712	F33	−0.1186	H44	0.1640

2. Molecular models and simulation methods

2.1. Molecular models

The systems studied consist of 2,2-bis(3,4-dicarboxyphenyl)-hexafluoropropane dianhydride (6FDA)/4,4′-diaminediphenyl-methane (MDA) polyimide (PI) [31], octahydrido silsesquioxane (OHS)/PI blends and octaaminophenyl silsesquioxane (OAPS)/PI

Table 3
Parameters used in HC force field [8,44] for OHS and OAPS.

E_b	b_0 (Å)	k_2 (kcal/mol Å^2)	k_3 (kcal/mol Å^3)	k_4 (kcal/mol Å^4)
Si–C	1.899	189.65	−279.42	307.51
Si–O	1.640	359.123	−517.342	673.707
Si–H	1.478	202.78	−305.36	280.27
C_{ar}–C_{ar}	1.417	470.836	−627.618	1327.635
C–H	1.0982	372.825	−803.453	894.317
C–N	1.400	350.0	0.0	0.0
N–H	1.031	540.112	−1500.295	2431.008
E_θ	θ_0 (deg)	H_2 (kcal/mol rad^2)	H_3 (kcal/mol rad^3)	H_4 (kcal/mol rad^4)
C–Si–O	114.9	23.0218	−31.3993	24.9814
O–Si–O	110.7	70.3069	−6.9375	0.0
Si–O–Si	159.0	8.500	−13.4188	−4.1785
H–Si–O	107.4	57.664	−10.6506	4.6274
C–C–Si	120.0	61.0	−35.0	0.0
C–C–H	117.94	35.1558	−12.4682	0.0
C–C–C	118.9	61.0226	−34.9931	0.0
C–C–N	120.0	60.0	0.0	0.0
E_ϕ		V_1 (kcal/mol)	V_2 (kcal/mol)	V_3 (kcal/mol)
Si–O–Si–O		−0.225	0.0	−0.010
Si–O–Si–H		0.0	0.0	−0.010
Si–O–Si–C		0.0	0.0	−0.010
H–C–C–H		0.0	2.35	0.0
Si–C–C–H		0.0	4.5	0.0
N–C–C–H		0.0	4.5	0.0
H–N–C–C		0.0	1.0	0.0
C_{ar}–C_{ar}–C_{ar}–C_{ar}		8.3667	1.2	0.0
E_{vdw}		r_{ij} (Å)	ε_{ij} (kcal/mol)	
Si–Si		4.405	0.198	
O–O		3.3	0.08	
H–H		2.878	0.0230	
C–C		3.915	0.068	
N–N		3.83	0.096	

Table 4
Partial charges for atoms in the POSS molecules.

Molecule	q_{Si}	q_O	H(–Si) q_H	H(–C) q_H	H(–N) q_H	q_N	q_C	
OHS	0.808	−0.529	−0.0134					
OHS [45]	1.93	−1.10	−0.28					
OAPS	0.876	−0.538		0.174	0.258	−0.544	C(–SiC–)	−0.204
							C(–CH–)	−0.165
							C(–CN–)	0.1043

blends. The chemical structure for the PI repeat unit is shown in Fig. 1. The molecular weight of the PI was 18196.4 g/mol, corresponding to an $n = 30$ monomer chain. The chemical structures for the two POSS species (OHS and OAPS) are shown in Fig. 2. The POSS cage has an edge length (Si to Si) of 3.14 Å. The cube's edge length (H to H) for OHS is about 4.8 Å, and the cube's edge length (N to N) for OAPS is about 10 Å.

The TRIPOS 5.2 force field [38] was used to model the atomic interactions in PI. This force field has been used to model polyimides and other polymers that have a large number of aromatic rings [39,40]. Physical properties that have been validated with the TRIPOS force field include cohesive energy, Hildebrand solubility parameters [39], and glass transition temperatures [40]. This force field consists of harmonic bond stretching (E_b), angle bending (E_θ), out-of-plane bending (E_χ), and torsion (E_ϕ) terms, which are shown in Eqs. (1)–(4), respectively.

$$E_b = k_{ij}\left(d_{ij} - d_{ij}^0\right)^2 \quad (1)$$

$$E_\theta = k_{jkj}(\theta - \theta_0)^2 \quad (2)$$

$$E_\chi = kd^2 \quad (3)$$

$$E_\phi = k_{ijkl}\left(1 + s/|s|{}^*\cos\left(|s|B_{ijkl}\right)\right) \quad (4)$$

where d_{ij} is the actual bond length, d_{ij}^0 is the equilibrium bond length, θ is the actual bond angle, θ_0 is the equilibrium bond angle, d is the distance from the atom to the plane defined by its three attached atoms, B is the torsion angle, k, k_{ij}, k_{jkj}, k_{ijkl} and s are the constants. The non-bonded interactions include the van der Waals and the electrostatic potentials. The 6-12 Lennard-Jones potential was used to model the van der Waals interaction.

$$u_{ij}(r) = 4\varepsilon_{ij}\left[\left(\frac{\sigma_{ij}}{r_{ij}}\right)^{12} - \left(\frac{\sigma_{ij}}{r_{ij}}\right)^{6}\right] \quad (5)$$

where ε_{ij} is the Lennard-Jones well-depth, σ_{ij} is the Lennard-Jones diameter, and r_{ij} is the distance between atoms i and j. The electrostatic potential is expressed by:

$$E_{coul} = \sum_{i,j}\frac{q_i q_j}{\varepsilon r_{ij}} \quad (6)$$

Table 5
Equilibrated box sizes for all systems at $T = 800$ K.

System	Equilibrated box sizes	Densities (g/cm^3)
1 Polyimide chain	30.56 Å × 33.34 Å × 27.79 Å	1.067
1 PI chain and 10.45 wt% OHS (5 OHS)	30.85 Å × 33.93 Å × 27.76 Å	1.161
1 PI chain and 5.96 wt% OAPS (1 OAPS)	34.92 Å × 32.01 Å × 26.19 Å	1.097
1 PI chain and 11.25 wt% OAPS (2 OAPS)	35.08 Å × 32.15 Å × 26.31 Å	1.147
1 PI chain and 20.23 wt% OAPS (4 OAPS)	42.60 Å × 31.24 Å × 25.56 Å	1.113

Table 6
Equilibrated box sizes for large systems at $T = 308$ K.

System	Box sizes
4 Polyimide chain	26.84 Å × 58.57 Å × 48.81 Å
4 PI chain and 10.45 wt% OHS (20 OHS)	27.76 Å × 61.07 Å × 49.97 Å
4 PI chain and 5.96 wt% OAPS (4 OAPS)	31.01 Å × 56.85 Å × 46.52 Å
4 PI chain and 11.25 wt% OAPS (8 OAPS)	31.69 Å × 58.10 Å × 47.54 Å
4 PI chain and 20.23 wt% OAPS (16 OAPS)	38.47 Å × 56.43 Å × 46.17 Å

where q_i is the partial charge on atom i, and ε is the dielectric constant. The parameters and constants for the TRIPOS force field used for this work are given in Table 1. The partial charges were obtained by first doing *ab initio* calculations in GAMESS [41] (General Atomic and Molecular Electronic Structure System) with the [6-31G(d)] [42] basis set to get the ESP (electrostatic potential) charges. As shown in Fig. 1b, we took one PI monomer and added part B to C1, and added part A to N23, and did the *ab-initio* calculations for [A-Monomer-B]. The R.E.D. (RESP ESP charge Derive) program [43] was then used to obtain the partial charges for the monomer fragment of the PI chain. These partial charges are listed in Table 2.

The Hybrid-COMPASS (HC) force field [8,44] was used to model the atomic interactions in OHS and OAPS. This force field includes bond stretching (E_b), angle bending (E_θ), and torsion (E_ϕ) terms which are described by Eqs. (7)–(9), respectively.

$$E_b = k_2(b - b_0)^2 + k_3(b - b_0)^3 + k_4(b - b_0)^4 \quad (7)$$

$$E_\theta = H_2(\theta - \theta_0)^2 + H_3(\theta - \theta_0)^3 + H_4(\theta - \theta_0)^4 \quad (8)$$

$$E_\phi = V_1(1 - \cos(\phi)) + V_2(1 - \cos(2\phi)) + V_3(1 - \cos(3\phi)) \quad (9)$$

where b_0 is the equilibrium bond length, θ_0 is the equilibrium bond angle, b is the actual bond length, θ is the actual angle, ϕ is the actual value of the dihedral angle, k_2, k_3, k_4, H_2, H_3, H_4, V_1, V_2, and V_3

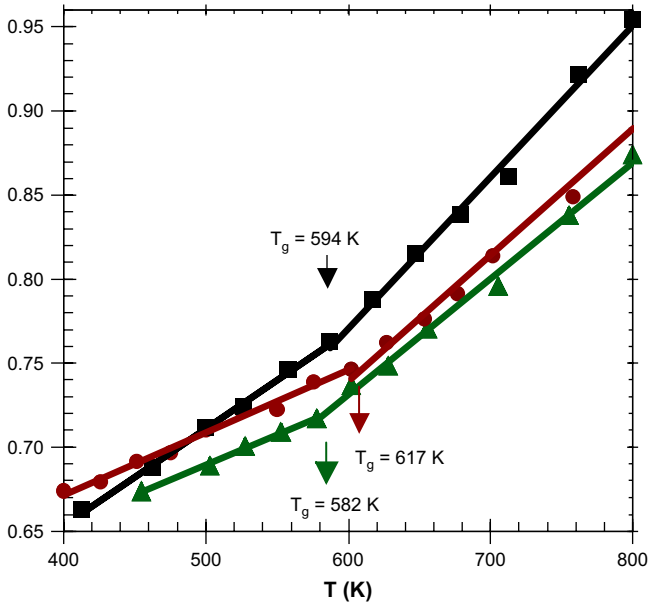

Fig. 3. Specific volume ($\langle v \rangle$) versus temperature for pure PI (black squares), PI and 20.23 wt% OAPS (dark red circles), PI and 10.45 wt% OHS (green triangles) at 1 atm obtained from NPT dynamics. The symbols indicate the state points calculated with MD simulation. The lines shown are least-squares linear regression fits through the data. The arrow indicates the position of the T_g from MD simulation. (For interpretation of the references to color in this figure legend, the reader is referred to the web version of this article.)

Table 7
Glass transition temperatures and specific volumes for POSS–PI blends at 1 atm.

wt% POSS, MD	T_g (K), MD	$\langle v \rangle$[a] (cm^3/g), MD
MD simulation results		
0	594	0.627
5.96 OAPS	606	0.638
11.25 OAPS	622	0.640
20.23 OAPS	617	0.644
10.45 OHS	582	0.631
wt% POSS, expt.	T_g[b] (K), expt.	$\langle v \rangle$[a,c] (cm^3/g), expt.
Experimental results		
0	570	0.725
5 OAPS	582	0.715
10 OAPS	591	0.713
20 OAPS	592	0.714
10 OHS	–	–

[a] Specific volumes at 300 K.
[b] Experimental data from Ref. [31].
[c] Iyer and Coleman, personal communication.

are constants. The Lennard-Jones (LJ) 9-6 function (E_{vdw}) was used to model the van der Waals interactions,

$$U_{vdw} = \varepsilon_{ij}\left\{2\left[\frac{r_{ij}}{r}\right]^9 - 3\left[\frac{r_{ij}}{r}\right]^6\right\} \quad (10)$$

where ε_{ij} is the LJ well-depth potential, r_{ij} is the effective LJ interaction diameter between atoms i and j, r is the actual distance of the atom pair.

$$r_{ij} = \left(\frac{r_i^6 + r_j^6}{2}\right)^{1/6} \quad (11)$$

$$\varepsilon_{ij} = \left(\frac{2r_i^3 r_j^3 \sqrt{\varepsilon_i \varepsilon_j}}{r_i^6 + r_j^6}\right) \quad (12)$$

where, r_i, r_j, ε_i, and ε_j represent the like atom interaction parameters for atoms i and j, respectively. Table 3 shows the Hybrid-COMPASS force field parameters used for this work. The non-bonded interaction terms include the Coulombic function (E_{coul}) for electrostatic interactions, which is shown in Eq. (6). In the HC force field, the partial charge q_i is given by:

$$q_i = \sum_j \delta_{ij} \quad (13)$$

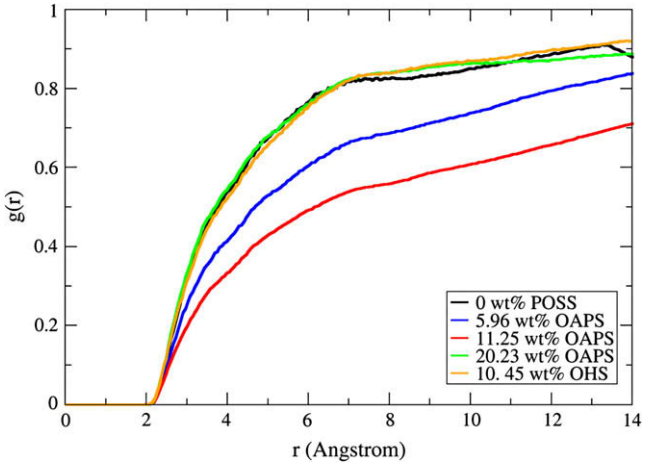

Fig. 4. Radial distribution function based on all atom of PI to all atom of PI for system with 0 wt% POSS, 10.45 wt% OHS, 5.96, 11.25, and 20.23 wt% OAPS at 308 K.

where δ_{ij} is the bond increment for an atom j that is valence bonded to atom i. However, in this work, the partial charges shown in Table 4 were obtained from *ab initio* calculations done in GAMESS [41] with [6-31G(d)] [42] basis set. Recently, Li et al. [45] reported partial charges for OHS and these are shown in Table 4 for comparison.

The LJ 6-12 potential and the electrostatic potential shown in Eqs. (5) and (6), respectively are also used to model the interactions between PI atoms and POSS atoms. We used Lorentz–Berthelot [46] combining rules: $\sigma_{ij} = (\sigma_i + \sigma_j)/2$ and $\varepsilon_{ij} = \sqrt{\varepsilon_i \varepsilon_j}$.

2.2. Molecular dynamics details

All molecular dynamics (MD) simulations were performed using the LAMMPS [47] (Large-scale Atomic/Molecular Massively Parallel Simulator) program. To begin, a single PI chain was placed into a large simulation box at a very low density. To achieve the proper density, MD simulations in the NPT (constant number of particles, pressure, and temperature) ensemble were conducted at 1 atm and 800 K. The Nose/Hoover thermostat [48] and barostat [48] were used to control the temperature and pressure, respectively. The velocity Verlet integrator was used to integrate the equations of motion. The time step used was 0.5 fs for pure PI and OHS/PI systems, and 0.2 fs for OAPS/PI systems. Cutoff radii of 10 Å and 11 Å were used for LJ and Coulombic interactions, respectively for all simulations. A particle–particle/particle–mesh Ewald (PPPM) algorithm [49] was used for the long-range Coulombic interactions. At 800 K, the single PI chain was relaxed until it formed a big coil in the simulation box. This relaxed PI chain was then used to start the simulation for each system. To make sure a system reached equilibrium, the simulation was initially conducted at 800 K for more than 1 ns. A number of thermodynamic quantities were monitored during equilibration; if they remained stable for more than 0.5 ns, it was concluded that the system was equilibrated. The resulting box sizes of the equilibrated configurations for all the systems are shown in Table 5.

After equilibration, production runs were used to observe the properties of polymer and mixed-matrix materials, such as glass transition temperature. The glass transition temperature of a polymeric material can be determined by plotting specific volume versus temperature at constant pressure and noting where the slope changes. The specific volume as a function of temperature was obtained by performing simulations in the NPT ensemble with the temperature range of 400–800 K and pressure of 1 atm. Each system was first equilibrated at a temperature of 800 K for about 1 ns, then the system was cooled to lower temperatures by decreasing the temperature by an increment of 25–50 K. For temperatures lower than 800 K, the system was run for 500 ps. For all systems, specific volumes reached equilibrium after 100–250 ps, depending on the temperature.

In addition to the glass transition temperatures, we have also calculated the intermolecular radial distribution functions for PI–PI, POSS–POSS, POSS–PI. The production runs for these cases considered larger systems which contain 4 PI chains. This large system was created by first cooling the system obtained from the glass transition temperature studies from 400 K to 325 K with 25 K intervals, and then from 325 K, it was again cooled to 308 K. At each temperature, the simulations were run for 500 ps. Then, at 308 K, we replicated twice the number of atoms in y and z directions, and ran the simulation for 2 ns in the NPT ensemble. To ensure that the structure that we obtained in the production run is in equilibrium, we compared the rdf plots after the simulation runs of 1 ns, 1.5 ns, and 2 ns. If the difference was smaller than 5%, then the structure was concluded to be at equilibrium. For the 20.23 wt% OAPS system,

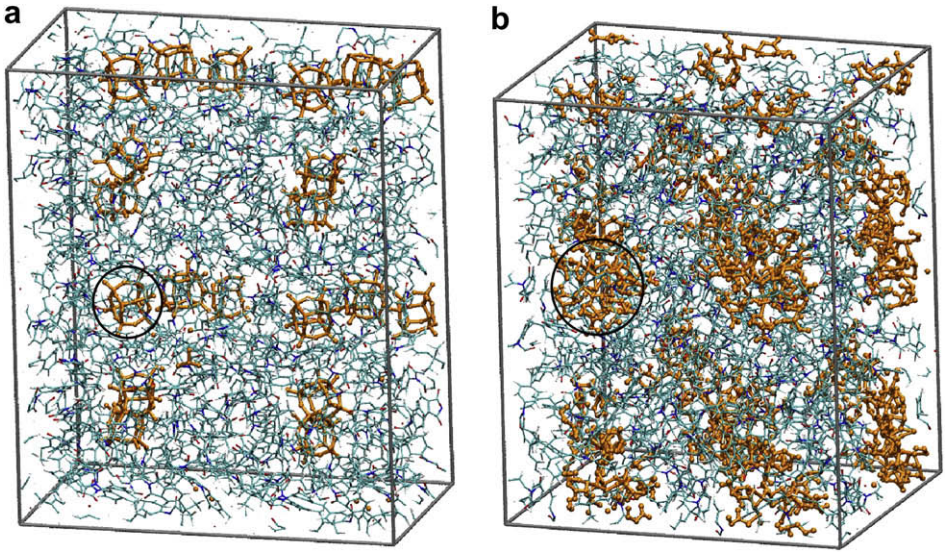

Fig. 5. Snapshot of POSS molecules (orange) and PI (a) 10.45 wt% OHS/PI blends at 308K, (b) 20.23 wt% OAPS/PI blends at 308 K. For clarity, a single POSS molecule is circled in each snapshot. Snapshots generated with Visual Molecular Dynamics (VMD) [55]. (For interpretation of the references to color in this figure legend, the reader is referred to the web version of this article.)

we found that the radial distribution function based on POSS to POSS did not reach equilibrium after the 2 ns run; another 1.5 ns of simulation time was needed to get an equilibrated radial distribution function.

We also calculated mean square displacement for PI and POSS. This calculation was done at 650 K. The production runs for this case considered large systems as well. The equilibrated system at 650 K obtained from glass transition temperature observation was used as the initial configuration. We then replicated twice of the number of atoms in *y* and *z* directions, and ran the simulation for about 1.5 ns in the NPT ensemble Table 6.

3. Results and discussion

3.1. Glass transition temperature

NPT molecular dynamics simulations were conducted at 1 atm to calculate the volume–temperature properties of the pure PI and PI–POSS blends. The uncertainty for the specific volume is in the range of 0.01–0.04 cm^3/g, in terms of the standard error calculated for the specific volume during the production run. The specific volume versus temperature plots are shown in Fig. 3 for PI, a blend of PI and 10.45 wt% OHS, and a blend of PI and 20.23 wt% OAPS. The temperature at which the slope changes on the specific volume–temperature plot represents the glass transition temperature (T_g) [16,50]. An arrow indicates the location of T_g. Simulations were also performed for a blend with 5.96 and 11.25 wt% OAPS. The standard error for the T_g calculation is ~9–15 K for different systems, which is based on the errors associated with the two least-squares linear regression fits of the specific volume versus temperature.

The glass transition temperatures and specific volumes for the pure PI and POSS–PI blends obtained from the simulations and experiments [31] are summarized in Table 7. The simulated glass transition temperatures are about 4% higher than the experimental values. The specific volumes for each system are reported at 300 K. For the pure PI and OAPS systems, the specific volumes obtained from the simulation are about 10% smaller than the experimental results. The experimental results shown in Table 7 were obtained using PI with the number-average molecular weight of 47,152, which is about twice more than the length of the PI chain considered in the current simulation work. In the literature [51,52], it has been shown that by varying the number of repeat units, the glass transition temperature of a polymer will shift. Additionally, the cooling rates used in the simulation are much higher (of order 10^{10} K/s) than experimental cooling rates. This is necessary due to computational limitations, which restrict the simulation to time-scales on the order of picoseconds [53]. It is known that a higher cooling rate may shift the glass transition temperature to a higher value [53,54]. Therefore, in this comparison, the simulation results are expected to agree qualitatively but not quantitatively to the experimental results.

The incorporation of OAPS has caused an increase of the T_g. Qualitatively, the model correctly reproduces the experimentally observed effect of increased OAPS loading up to 11 wt% on T_g. Namely, that the glass transition temperature gradually increases up to that weight percent of OAPS [31] and then remains constant beyond 10 wt% of OAPS, up to 30 wt% [31]. While simulation results show a slight decrease of the T_g after the addition of 20 wt% OAPS, this decrease is within the bounds of uncertainty and not significant.

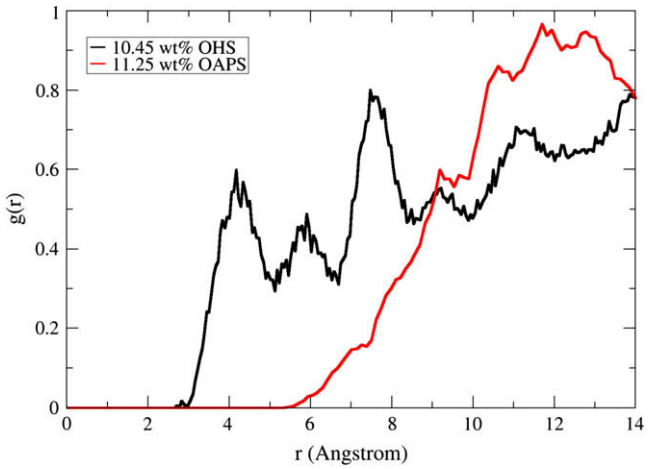

Fig. 6. Radial distribution function based on POSS to POSS (Si and O atom types) for system with 10.45 wt% OHS and 11.25 wt% OAPS at 308 K.

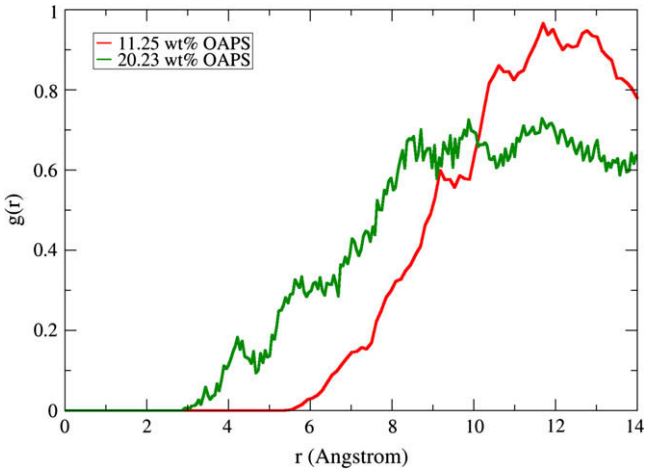

Fig. 7. Radial distribution function based on POSS to POSS (Si and O atom types) for system with 11.25 wt% OAPS and 20.23 wt% OAPS at 308 K.

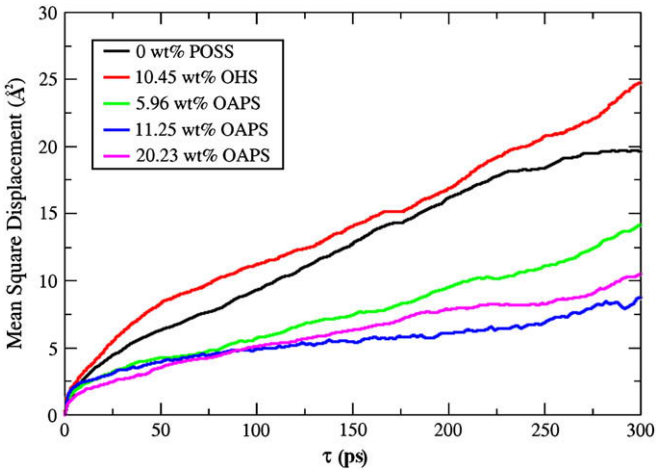

Fig. 9. Mean square displacement of the PI chains for all systems at $T = 308$ K.

The T_g value for system containing 10.45 wt% OHS blended with PI is lower than the T_g value for the pure PI. This reduction in T_g is expected because OHS (hydrogen-functionalized POSS) is known to be incompatible with PI. We are not aware of experimental data for OHS/PI blends. Similar reduction in T_g was observed for octaphenyl-POSS (OPS)/PI blends in experiments by Iyer and Coleman [31]. They observed unfavorable interactions between OPS and PI which suggested the incompatibility of these two species.

To check the effects of system size on the glass transition temperature determination, we compared the specific volume obtained from the small systems (containing 1 PI chain) at 308 K to the specific volume obtained from the large systems (containing 4 PI chains) at 308 K. The results are comparable with the difference of the values less than 1%.

3.2. Radial distribution functions

The radial distribution function (rdf), $g(r)$ provides more understanding of the POSS and polymer packing details. As mentioned before, the simulations conducted to calculate the rdfs contained 4 PI chains. These systems were larger to obtain better statistics for the rdf analysis. In this section, we present rdfs for PI–PI, POSS–POSS, and POSS–PI. Fig. 4 shows the intermolecular packing, $g(r)$ based on all atom centers of PI to PI in the systems. The $g(r)$ has a lower value with the incorporation of 5.96 and 11.25 wt% OAPS compared to the one with 0 wt% POSS. This indicates that with the incorporation of OAPS up to 11.25 wt%, the presence of OAPS decreased the density of contacts between PI to PI. On the other hand, the incorporation of 20.23 wt% OAPS shows that the density of contacts between PI to PI is the same as for 0 wt% POSS. This indicates that the incorporation of 20.23 wt% OAPS may have caused the PI polymers to start to cluster together and phase separate from the POSS. The $g(r)$ for 10.45 wt% OHS also suggests that the PI has phase separated from the POSS.

The intermolecular packing of POSS to POSS based on the Si and O atoms in polymeric system is shown in Figs. 6 and 7. Fig. 6 compares the $g(r)$ for system with 10.45 wt% OHS to the $g(r)$ for system with 11.25 wt% OAPS at $T = 308$ K. The $g(r)$ data for OHS indicate that there are distinct peaks at around $r = 4.0$, 6.0, and 7.5 Å. These peaks are direct evidence that there is a specific organization of the neighboring OHS molecules in PI system, indicating that aggregation of OHS has occurred. The aggregation can also be seen in the snapshot shown in Fig. 5(a). It has been stated that POSS molecules tend to crystallize at room temperature [29,56]. Zheng et al. [56] observed that aggregation and crystallization occurred for octaisobutyl-POSS within polysiloxane

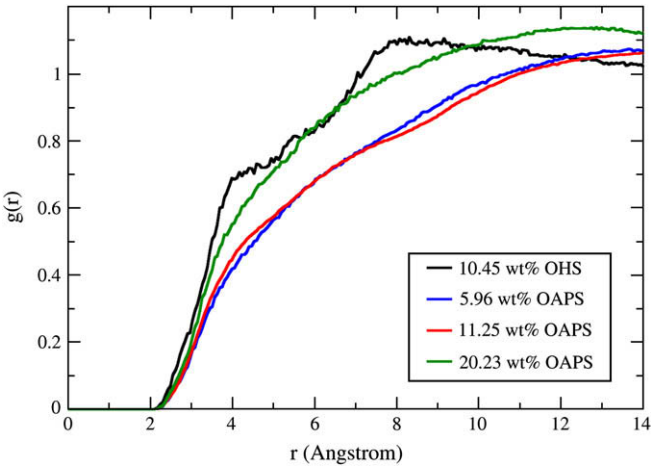

Fig. 8. Radial distribution function based on all-atom POSS to all-atom polyimide for system with 10.45 wt% OHS, 5.96 wt% OAPS, 11.25 wt% OAPS, and 20.23 wt% OAPS at 308 K.

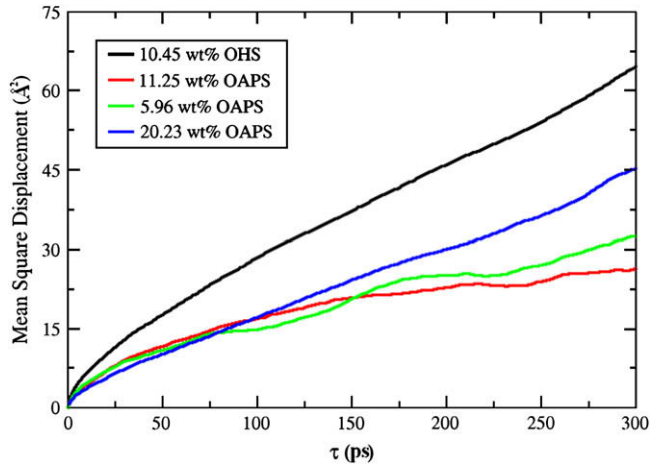

Fig. 10. Mean square displacement of the POSS molecules for system with 5.96 wt% OAPS, 11.25 wt% OAPS, and 20.23 wt% OAPS at $T = 308$ K.

elastomer. However, the short simulation time duration used here makes it impossible to observe any tendency of spontaneous crystallization of POSS. On the other hand, the $g(r)$ data for 11.25 wt% showed that the OAPS–OAPS contacts started to show only at the distance of 5.5 Å. There are no distinct peaks shown in the plot, which means a weak, liquid like ordering structure of OAPS molecules. Fig. 7 shows the comparison of the rdf plots for POSS with different loadings of OAPS. The data from 5.96 wt% OAPS is not shown because the OAPS molecules are more dilute in the PI system, and therefore did not exhibit any aggregation on the time scale of the simulation. For the 11.25 and 20.23 wt% OAPS, both plots indicate featureless coordination of OAPS within the PI system, which means a good dispersion of OAPS. This can be also seen in the snapshot shown in Fig. 5(b).

Fig. 8 shows the intermolecular packing of the PI polymer chains around the POSS at $T = 308$ K. The rdf shown is based on all atom polyimide chain to all atom POSS. The plot shows some diffuse peaks for system with 10.45 wt% OHS at $r \sim 4$ Å and 8 Å, which means that the packing of PI to OHS is more structured than the packing of PI to OAPS. The geometry of the POSS cage, composed of Si and O atoms is highly constrained and only capable of small deformation [16]. Therefore, the main difference between OAPS and OHS is in the way that the substituents (aminophenyl groups or hydrogen atoms) pack around the POSS cage. Since there are only hydrogen atoms as the functional groups on the OHS molecule, OHS can pack more compactly, which allows the polymer chains to approach closer to the OHS. The plot for 10.45 wt% OHS system shows the highest $g(r)$ at almost all distances less than 9.7 Å. This means that the density of PI–OHS contacts is higher compared to density of PI–OAPS contacts. For different loadings of OAPS, the highest density of PI–OAPS contacts occurred for the system with 20.23 wt% OAPS. There is no much difference of how the PI chain packed around the POSS molecules for low loading (5.96 wt% and 11.25 wt%) of OAPS.

Experimental studies have shown that the increase of T_g due to the incorporation of POSS can be because of two aspects: (i) when POSS increases the interaction contacts between POSS to polymer chain [31,57–59] i.e., a good dispersion of POSS in the polymer system, and (ii) when the relatively rigid POSS molecules retard the motion of the polymer [31,57,60]. Iyer et al. [31] also noted that T_g may decrease if phase separation takes place. From the radial distribution functions based on POSS to POSS, aggregation occurred for OHS molecules. In addition, Fig. 4 has shown there is no effect on PI to PI contacts after the addition of OHS molecules in the system. This means that the PI polymer chains were still clustering together. These two facts indicate that phase separation might have occurred and caused the lower T_g for this blend. The rdfs for OAPS systems based on POSS to POSS showed that OAPS molecules do not have the tendency to aggregate. Fig. 4 has also shown a decrease of PI to PI interaction contact for low loading (5.96 wt% and 11.25 wt%) of OAPS. These indicate that OAPS molecules were well dispersed in the systems. Our simulation results have shown there was a gradual increase in T_g as the OAPS loading increased up to 11.25 wt%. In the following section, the effect of POSS on the mobility of the PI chain will be discussed.

3.3. Mobility of PI and POSS

To observe the mobility of PI chains in the nanocomposite materials, the mean square displacements (MSD) were calculated at a temperature above the glass transition temperature, 650 K. Fig. 9 shows the MSD plots for PI for all cases. The MSD are calculated based on the center of mass of each polyimide chain and averaged over the 4 chains. The presence of POSS molecules on PI polymeric system was expected to affect the mobility of the polymer chain [31]. The mobility of PI chain decreased with the incorporation of OAPS, on the other hand, the mobility increased slightly with the incorporation of OHS. These observations agree with the glass transition temperature results, which showed an increase of the T_g after the incorporation of OAPS, and a decrease of the T_g after the incorporation of OHS. The least steep slope of MSD for PI is found for 11.25 wt% OAPS system. This indicates that the mobility of the PI chains was the slowest for this system.

Besides the mobility of PI chains, we have also observed the mobility of POSS molecules at $T = 650$ K. Fig. 10 shows the mean square displacement plot for POSS molecules in PI polymer chains. The MSD calculations consider multiple origins separated by 2.0 ps and they are averaged over all POSS molecules in each system. It is shown that the MSD for OHS molecules is higher compared to the MSD for OAPS at all times. The smaller size and the compact structure of OHS allow it to move more in the PI system compared to the OAPS. The aminophenyl groups in OAPS decrease the motion of the POSS molecules in the polymeric matrix. The slope of the MSD plot for 11.25 wt% system is the least steep one. This means that OAPS for this system has the slowest motion compared to the other systems. Our glass transition temperature results showed that the T_g for system with 11.25 wt% OAPS was the highest. These observations support our glass transition temperature results discussed earlier. If the addition of POSS molecules retards the motion of the species in a nanocomposite, the glass transition temperature will increase. In addition to that, the aminophenyl group has been known to improve the compatibility of POSS to the PI chain [31]. The compatibility of these two species will make them interact more favorable, and therefore retard the motion of both species.

4. Conclusions

The effect of incorporating POSS to the polyimide polymer matrix has been explored with atomistic molecular dynamics simulations. The specific volume versus temperature plots were obtained from simulations to determine the glass transition temperatures. The glass transition temperatures obtained from simulations agree qualitatively to the results obtained from experiment. The blending of OAPS into the PI matrix showed an increase of the glass transition temperatures. An increase of up to 11.25 wt% of OAPS increases the glass transition temperatures of the materials. On the other hand, the blending of OHS into the PI matrix showed a decrease of the glass transition temperature.

From the radial distribution functions calculations, it was shown that the density of PI–OHS contacts is higher compared to the density of PI–OAPS contacts. PI chains packed more efficiently around OHS than around OAPS. This is due to the more compact structure and the much denser molecule of OHS compared to OAPS. The OHS molecules arranged in a more ordered fashion compared to the OAPS molecules in nanocomposite materials. Radial distribution functions plots also show the liquid like ordering structure of OAPS molecules in the polymeric system.

The mobility of PI chains and POSS molecules was observed by the mean squared displacements. The incorporation of OAPS has reduced the mobility of polyimide. However, the incorporation of OHS has slightly increased the mobility of polyimide chains.

Our simulation results have shown the behavior of POSS in PI polymer matrix. PI is a rigid polymer. For future study, a flexible backbone polymer, poly(dimethylsiloxane), PDMS, will be considered. This flexible polymer is expected to allow more loading of POSS. Our current results have shown that the incorporation of OAPS increased the glass transition temperature of the nanocomposite materials. Another motivation will be also to consider the PI–PDMS copolymer. This copolymer will combine the advantage of PI (high glass transition temperature) and the flexibility of

PDMS which may then lead to a copolymer that can withstand elevated temperature and therefore can be used for applications, such as membranes for gas separation.

Acknowledgments

This work was supported by the Department of Chemical and Biological Engineering at Iowa State University. The computational work was performed at the ISU High Performance Computing facility.

References

[1] Paul DR, Yampol'skii YP. Polymer gas separation membranes: introduction and perspective. CRC Press; 1994.
[2] Zimmerman CM, Singh A, Koros WJ. J Membr Sci 1997;137:145–54.
[3] Dodiuk H, Rios PF, Dotan A, Keniq S. Polym Adv Technol 2007;18:746–50.
[4] Oaten M, Choudhury NR. Macromolecules 2005;38:6392–401.
[5] Devaux E, Rochery M, Bourbiqot S. Fire Mater 2002;26:149–54.
[6] Laine RM. J Mater Chem 2005;15:3725.
[7] Peng Y, McCabe C. Mol Phys 2007;105:261.
[8] Ionescu TC, Qi F, McCabe C, Striolo A, Kieffer J, Cummings PT. J Phys Chem B 2006;110:2502.
[9] Pielichowski K, Njuguna J, Janowski B, Pielichowski J. Adv Polym Sci 2006;201:225–96.
[10] Striolo A, McCabe C, Cummings PT. J Phys Chem B 2005;109:14300.
[11] Agaskar PA. Inorg Chem 1991;30:2707.
[12] Laine RM, Zhang C, Sellinger A, Viculis L. Appl Organomet Chem 1998;12:715.
[13] Striolo A, McCabe C, Cummings PT. Macromolecules 2005;38(21):8950–9.
[14] Striolo A, McCabe C, Cummings PT, Chan ER, Glotzer SC. J Phys Chem B 2007;111(42):12248–56.
[15] Striolo A, McCabe C, Cummings PT. J Chem Phys 2006;125:104904.
[16] Bharadwaj RK, Berry RJ, Farmer BL. Polymer 2000;41:7209.
[17] Lichtenhan JD. Comments Inorg Chem 1995;17:115–30.
[18] Mark JE. Macromol Symp 2003;201:77–83.
[19] Li GZ, Wang LC, Ni HL, Pittman Jr CU. J Inorg Organomet Polym 2001;11:123–54.
[20] Schwab JJ, Lichtenhan JD. Appl Organometal Chem 1998;12:707–13.
[21] Lee YJ, Huang JM, Kuo SW, Lu JS, Chang FC. Polymer 2005;46:173–81.
[22] Leu CM, Chang YT, Wei KH. Chem Mater 2003;15:3721–7.
[23] Chen YW, Kang ET. Mater Lett 2004;58:3716–9.
[24] Mather PT, Jeon HG, Romo-Uribe A. Macromolecules 1999;32:1194–203.
[25] Lichtenhan JD, Otonari YA, Carr MJ. Macromolecules 1995;28:8435–7.
[26] Romo-Uribe A, Mather PT, Haddad TS, Lichtenhan JD. J Polym Sci Part B Polym Phys 1998;36:1857–72.
[27] Haddad TS, Lichtenhan JD. Macromolecules 1996;29:7302.
[28] Kim KM, Keum DK, Chujo Y. Macromolecules 2003;36:867–75.
[29] Liu L, Tian M, Zhang W, Zhang LQ, Mark JE. Polymer 2007;48:3201–12.
[30] Liu L, Hu Y, Song L, Nazare S, He SQ, Hull R. J Mater Sci 2007;42:4325–33.
[31] Iyer P, Coleman MR. J Appl Polym Sci 2008;108:2691–9.
[32] Xu H, Kuo JW, Lee JS, Chang FC. Macromolecules 2002;35:8788–93.
[33] Fu BX, Hsiao BS, Pagoda S, Stephens P, White H, Rafailovich M, et al. Polymer 2001;42:599.
[34] Zheng L, Farris RJ, Coughlin EB. Macromolecules 2001;34:8034–9.
[35] Capaldi FM, Rutledge GC, Boyce MC. Macromolecules 2005;38:6700–9.
[36] Patel RR, Mohanraj R, Pittman Jr CU. J Polym Sci Part B Polym Phys 2006; vol. 44:234–48.
[37] Chan ER, Striolo A, McCabe C, Cummings PT, Glotzer SC. J Chem Phys 2007;127:114102.
[38] Clark M, Cramer III RD, Opdenbosch NV. J Comput Chem 1989;10:982–1012.
[39] Pinel E, Brown D, Bas C, Mercier R, Alberola ND, Neyertz S. Macromolecules 2002;35:10198–209.
[40] Qi D, Hinkley J, He G. Modell Simul Mater Sci Eng 2005;13:493–507.
[41] Schmidt MW, Baldridge KK, Boatz JA, Jensen JH, Koseki S, Matsunaga N, et al. J Comput Chem 1993;14:1347.
[42] (a) Hehre WJ, Ditchfield R, Pople JA. J Phys Chem 1972;56:2257;
(b) Francl MM, Pietro WJ, Hehre WJ, Binkley JS, Gordon MS, Defrees DJ, et al. J Chem Phys 1982;77:3654;
(c) Clark T, Chandrasekhar J, Spitznagel GW, Schleyer PVR. J Comput Chem 1983;4:294;
(d) Frisch MJ, Pople JA, Binkley JS. J Chem Phys 1984;80:3265;
(e) Okuno Y. J Chem Phys 1996;105:5817.
[43] Pigache A, Cieplak P, Dupradeau FY. Automatic and highly reproducible RESP and ESP charge derivation: application to the development of programs RED and X RED. In: 227th ACS National Meeting, Anaheim, CA, USA; March 28–April 1, 2004.
[44] Sun H. J Phys Chem B 1998;102:7338–64.
[45] Li HC, Lee CY, McCabe C, Striolo A, Neurock M. J Phys Chem A 2007;111(18):3577–84.
[46] Allen MP, Tildesley DJ. Computer simulation of liquids. Oxford: Clarendon; 1987.
[47] Plimpton SJ. J Comput Phys 1995;117:1–19.
[48] Frenkel D, Smit B. Understanding molecular simulation. 2nd ed.; 2002.
[49] Hockney R, Eastwood J. Computer simulations using particle. New York: Adam Hilger; 1988.
[50] Nicholson JW. The chemistry of polymers. 3rd ed.; 2006.
[51] Fox TG, Flory PJ. J Appl Phys 1950;21:581–91.
[52] Zhang J, Liang Y, Yan JZ, Lou JZ. Polymer 2007;48:4900–5.
[53] Soldera A, Grohens Y. Macromolecules 2001;35(3):722–6.
[54] Bizet S, Galy J, Gerard JF. Polymer 2006;47:8219–27.
[55] Humphrey W, Dalke A, Schulten K. VMD – visual molecular dynamics. J Mole Graphics 1996;14:33–8.
[56] Zheng L, Waddon AJ, Farris RJ, Coughlin EB. Macromolecules 2002;35:2375.
[57] Huang JC, He CB, Xiao Y, Mya KY, Dai J, Siow YP. Polymer 2003;44:4491–9.
[58] Wahab MA, Kim I, Ha CS. Polymer 2003;44:4705.
[59] Xiong M, You B, Shuxue Z, Limin W. Polymer 2004;45:2967.
[60] Lee A. Mater Res Soc Symp Proc 1999;576:343–50.